Korean J. Chem. Eng., 33(2), 481-489 (2016)
DOI: 10.1007/s11814-015-0172-1

pISSN: 0256-1115
eISSN: 1975-7220

Adsorption and photocatalytic degradation of organic dyes onto crystalline and amorphous hydroxyapatite: Optimization, kinetic and isotherm studies

Solmaz Valizadeh, Mohammad Hossein Rasoulifard†, and Mir Saeed Seyed Dorraji

Applied Chemistry Research Laboratory, Department of Chemistry, Faculty of Science, University of Zanjan, Zanjan, Iran
(*Received 3 March 2015 • accepted 4 August 2015*)

Abstract−We evaluated the adsorptive/photodegradation properties of hydroxyapatite. Hydroxyapatite was synthesized by two different precipitation methods and examined for the removal of two kinds of textile dye. The physicochemical properties of the products were characterized using Fourier transform infrared, X-ray diffraction, inductively coupled plasma atomic emission spectroscopy and scanning electron microscopy. The effects of different parameters, including hydroxyapatite synthesis method and removal process type, pH, reaction time, temperature and amount of hydroxyapatite, were investigated and optimized by Taguchi design. The kinetics of adsorption and isotherm studies showed that the pseudo-second-order model and the Freundlich isotherm were the best choices to describe the adsorptive behavior of hydroxyapatite. Photocatalytic degradation of dye followed Langmuir-Hinshelwood mechanism, illustrated a pseudo-first-order kinetic model with the adsorption equilibrium constant and kinetic rate constant of surface reaction equal to 0.011 (l mg^{-1}) and 1.3 (mg l^{-1} min^{-1}), respectively.

Keywords: Hydroxyapatite, Crystalline, Amorphous, Dye, Adsorption, Photodegradation

INTRODUCTION

The increasing levels of hazardous dyes in wastewater due to industrial activities have been identified as a serious environmental issue worldwide. Many dyes and pigments contain aromatic rings in their structures, which make them toxic, non-biodegradable, carcinogenic, and mutagenic for aquatic systems and human health [1]. Recently, considerable interest has been focused on the elimination of toxic dyes from industrial effluents before being discharged into the water bodies [1,2]. The dyestuff contamination even at a very low concentration is visible, and the elimination of these dyes from wastewaters has major importance to human beings and aquatic organisms [3]. Various physical and chemical treatment methods, such as electrochemical techniques, ion exchange, adsorption and photocatalytic degradation, have been utilized for the elimination of residual dyes from wastewaters [4-7]. Among these processes, adsorption is one of the methods that has been successfully applied for dye removal from hazardous wastes due to low maintenance costs, high efficiency and ease of operation [8]. Along with adsorption, photocatalytic degradation has also emerged as an important destructive technology for total mineralization of the most of organic pollutants [9-11].

In recent years Hydroxyapatite (HAP, $Ca_{10}(PO_4)_6(OH)_2$), as one of the major mineral constituents of vertebrate bone and tooth, is the most well-known bioceramic from the apatitic family [12]. HAP has been used extensively in such fields as bone repairs, bone implant and bioactive materials [13,14]. Excellent biocompatibility, slow biodegradation, good mechanical stability, great sorption property and photocatalytic degradation activity under UV irradiation are novel aspects of HAP in environmental performance [15-17]. Photocatalytic activity of HAP under UV irradiation would be due to photo-induced electronic excitation and could be well explained by changing the electronic state of the surface PO_4^{3-} group and creation of electron vacancy on the surface of HAP. Produced electron is transferred to the surrounding oxygen followed by the formation of $O_2^{\bullet-}$ radicals. The generated superoxide radicals are very active in oxidizing organic compounds by reacting with the water molecules and $^-$OH ions and producing hydrogen peroxide. Consequently, $^\bullet$OH radicals will be produced which are also oxidizing the organic pollutants.

According to the previous studies, structure, crystallinity, particle size and morphology are some efficient factors which could affect the performance of HAP in contamination removal processes [18]. In the present work, to obtain a direct and comprehensive understanding of the adsorption and degradation properties of HAP, two different morphologies of HAP were synthesized by precipitation method. Direct Red 23 (DR23) and Acid Blue 25 (AB25) were selected as two different types of organic dyes. The effects of different parameters such as HAP synthesis method, type of removal process, pH, temperature, reaction time and amount of HAP were investigated by Taguchi experimental design. The kinetic models and isotherm equations were investigated by fitting the experimental data to various kinetic and isotherm models for the adsorption and photocatalytic degradation of DR23 and AB25.

EXPERIMENTAL

1. Materials and Instruments

Calcium nitrate tetrahydrate ($Ca(NO_3)_2)\cdot 4H_2O$ was obtained from Merck and Ammonium phosphate ($(NH_4)_2HPO_4$) was supplied

†To whom correspondence should be addressed.
E-mail: m_h_rasoulifard@znu.ac.ir, m_h_rasoulifard@yahoo.com

Table 1. Taguchi parameters and levels along with statistical analysis

Factor	Description	Level 1	Level 2	Level 3	Level 4	Dye	SS	P (%)
A	Type of removal process	C-HAP-UV	C-HAP	A-HAP-UV	A-HAP	DR23	19.5	62.8
						AB25	15673.4	55.4
B	pH	3	5	7	9	DR23	2.6	8.4
						AB25	3185.9	11.2
C	Reaction time (min)	15	30	60	90	DR23	0.6	18.9
						AB25	3270.8	11.5
D	Temperature (°C)	25	35	45	55	DR23	5.9	18.9
						AB25	2573.5	9.0
E	Amount of HAP (mg/*l*)	0.6	0.8	1.0	1.2	DR23	2.5	8.0
						AB25	3575.5	12.6

by Fluka. All of the other chemicals were analytical grade and used without further purification. UV-Vis spectrophotometer (Shimadzu 1650PC) was used for determining dye concentration. X ray diffraction (XRD) patterns of the prepared HAPs were analyzed by Siemens D-5000 diffractometer with Cu Kα radiation (Germany). The analysis was performed at 2θ ranging from 4 to 70 at a scanning speed of 1 min^{-1}. The Fourier transform infrared (FT-IR) spectra of the samples were recorded by Bruker Tensor 27 spectrometer over the wave number range of 4,000-400 cm^{-1}. While the morphology was studied by field emission scanning electron microscopy (FESEM, HITACHI S-109, 4160), the chemical composition of the synthesized samples was analyzed by inductively coupled plasma atomic emission spectroscopy (ICP-AES model Perkin Elmer1100 DV).

2. Synthesis of HAPs

Appropriate amount of aqueous solution (50 ml) containing 1.77 g $Ca(NO_3)_2{\cdot}4H_2O$ adjusted to pH 10 by adding ammonia solution, was added dropwise into a 50 ml aqueous solution with 1.74 g $(NH_4)_2HPO_4$ over 30 min with continuous mechanical stirring (1,100 rpm). Then the solution was heated to 90 °C for 2 h; the mixture was cooled to room temperature and aged overnight. The precipitation was filtered and washed twice with deionized water until neutral pH. The product was dried at 90 °C. Finally, the as-prepared sample was calcined at 400 °C for 3 h [19]. The synthesized hydroxyapatite was named Crystalline HAP (C-HAP).

Amorphous HAP (A-HAP) was also synthesized by precipitation procedure. At first, calcium nitrate solution (1.77 g Ca $(NO_3)_2{\cdot}4H_2O$ in 50 ml of distilled water) was immediately poured into diammonium hydrogen phosphate solution (1.74 g $(NH_4)_2HPO_4$ in 50 ml of distilled water). The pH of solution was adjusted to 7 by ammonia solution. After mild agitation for about 2 h, the suspension was filtered on a Buchner funnel and washed with distilled water and subsequently dried at 70 °C for about 48 h [15].

3. Procedures for Adsorption and Degradation

To study the adsorption and degradation properties of synthesized HAPs, DR23 and AB25 as two kinds of textile dyes were selected. A UV-C lamp (30 W, manufactured by Philips, Holland) was used as the source of UV irradiation. Different samples and experimental conditions were obtained by Taguchi L_{16} orthogonal array. The treated solutions were subsequently centrifuged (6,000 rpm) to measure the final dye concentration. Dye removal efficiency (R) was measured by UV-Vis spectrophotometry and calculated as Eq. (1):

$$R\% = 1 - \frac{C}{C_o} \times 100\% \quad (1)$$

where, C_o and C are the initial and final concentration of dye in the solution ($mg{\cdot}l^{-1}$), respectively.

4. Experimental Design

Among the experimental design methods, Taguchi method has become popular due to its systematic, simple and efficient approach for the optimization of the process parameters. This approach uses a special design of an orthogonal array to study all the factors with a small number of experiments [20]. This investigation was aimed to determine optimum process conditions for removal of DR23 and AB25 dyes by synthesized HAPs. The experimental parameters affecting the removal of dye and their levels are given in Table 1. Qualitek-4 software was used to design and analyze the most suitable experiments according to L_{16} orthogonal array. To observe the effects of noise sources on the dye removal, each experiment was carried out three times under the same conditions. The performance statistics was chosen as the optimization criterion. There are three categories of performance statistics: the larger-the-better, the smaller-the-better and the nominal-the-better. Because the target of this study is to maximize the pollutant removal efficiency, the S/N ratio with the -larger -the- better characteristics is required, which is given by Eq. (2)

$$\frac{S}{N} = -10 \log\left[\frac{1}{n}\sum\left(\frac{1}{R}\right)^2\right] \quad (2)$$

where n is the number of repetitions under the same experimental conditions, and R represents the results of measurements [21].

RESULT AND DISCUSSION

1. Characterization

The FT-IR spectra (Fig. 1) showed peaks located at 3,544 cm^{-1} and 630 cm^{-1}, both assigned to apatitic OH^- ions. The peaks at 3,488 and 1,600 cm^{-1} are related to stretching and bending modes of water -OH on the HAP surface. Surface adsorbed water on HAP is desorbed below 200 °C and desorption above 200 °C is assumed to be due to structural water of HAP [22]. According to the calcina-

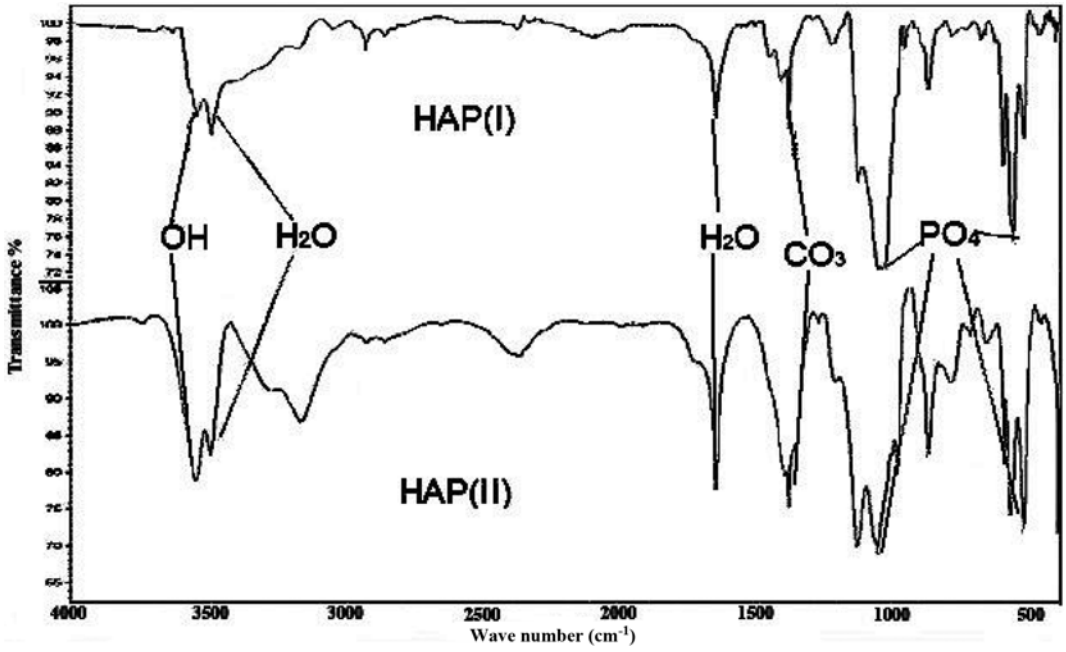

Fig. 1. FT-IR spectra of A-HAP and C-HAP.

tion temperature of C-HAP (400 °C), both surface adsorbed water and part of structural water in HAP would be desorbed, which appeared in the spectra with decreasing trend. Typical apatitic phosphate modes can be observed at 565 cm^{-1} and 1,040 cm^{-1} which exist in both synthesized HAP samples. The phosphate stretching bond occurring at 962 cm^{-1} indicates the crystalline structure of the apatite phase formation [23], which is observed only in C-HAP. In case of A-HAP the peaks at 1,142-1,209 cm^{-1} are representative of apatitic HPO_4^{2-}, which indicates the non-stoichiometry of the synthesized A-HAP. The appearance of CO_3^{2-} peak at 1,380 cm^{-1} is possibly due to the incorporation of CO_3^{2-} ions in the OH^- sites. This is because of alkaline condition in synthesis where enough OH^- ions are present in the aqueous system to react with the atmospheric CO_2 [19].

X-ray diffraction patterns of the HAPs are shown in Fig. 2. For A-HAP reflections characteristic of poorly crystalline apatite similar to bone mineral [15], no extra crystalline phase was detected. The broad and overlapping reflection of A-HAP confirmed the low crystallinity of hydroxyapatite. There were numerous sharp peaks in the XRD pattern of C-HAP. Meanwhile, the XRD pattern of the sample did not reveal any impurity; the sharp diffraction peaks indicated the synthesized C-HAP is well crystallized. The crystallinity degree, X_c, corresponding to the fraction of crystalline phase present in the examined volume, was evaluated by Eq. (3).

$$X_c = \left[1 - \left(\frac{V_{112/300}}{I_{300}}\right)\right] \quad (3)$$

where I_{300} is the intensity of the (300) diffraction peak and $V_{112/300}$ is the intensity of the hollow between (112) and (300) diffraction peaks [24].

While the A-HAP was the sample of amorphous hydroxyapatite, crystallinity degree of C-HAP was calculated 0.32.

The as-prepared HAPs were dissolved in nitric acid and analyzed by inductively coupled plasma-atomic emission spectroscopy (ICP-AES) to determine the Ca/P molar ratio. The 1.66 Ca/P molar ratio for C-HAP and 1.51 for A-HAP revealed that C-HAP syn-

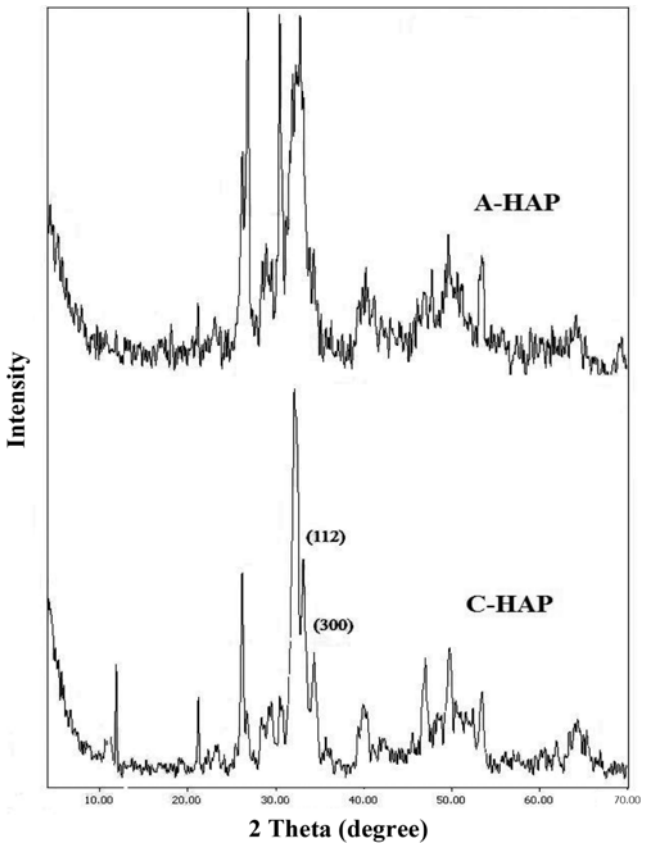

Fig. 2. XRD patterns of A-HAP and C-HAP.

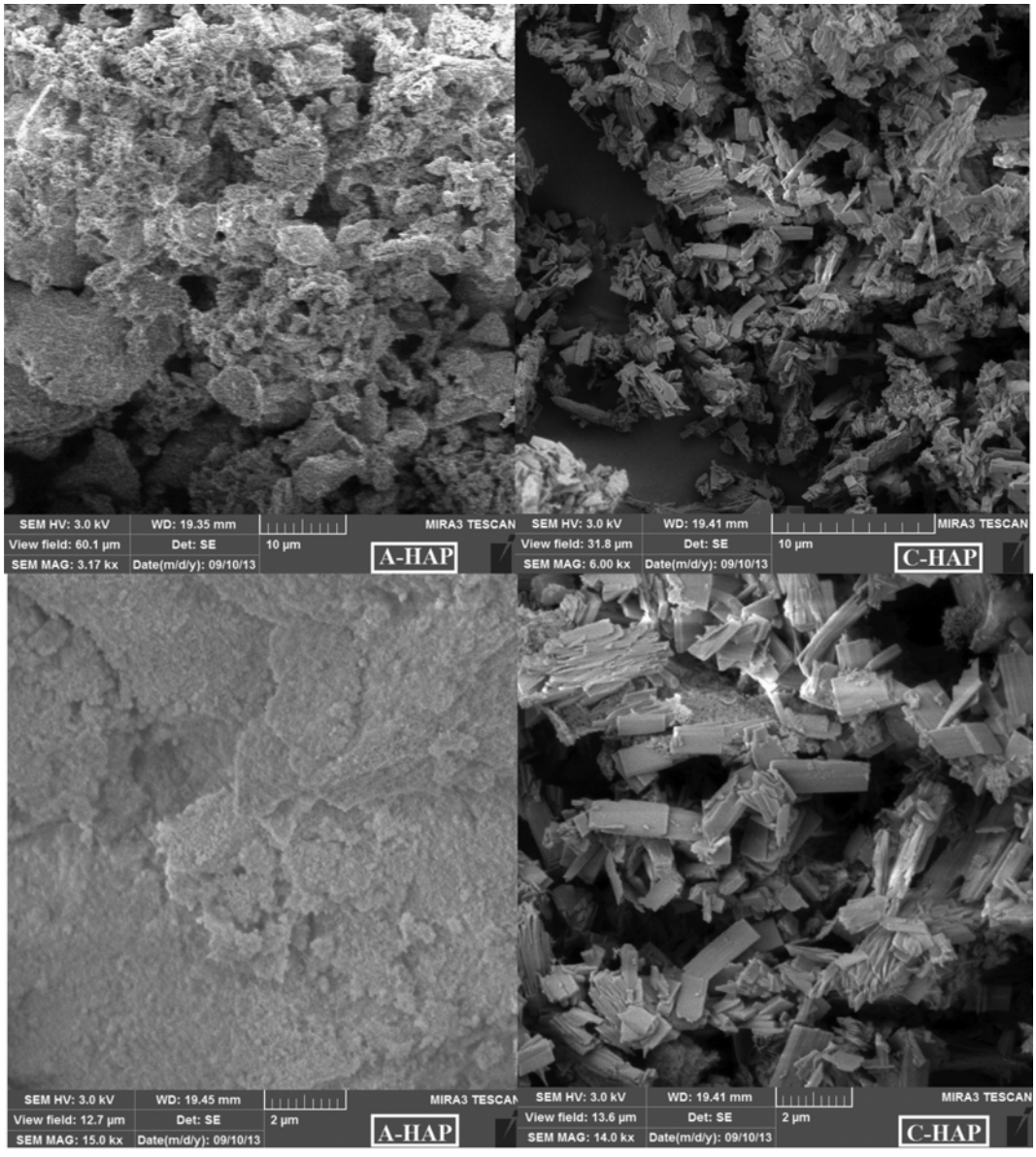

Fig. 3. FESEM images of A-HAP and C-HAP.

thesize stoichiometrically and the Ca/P ratio for A-HAP is lower than that of stoichiometric hydroxyapatite (1.67). These findings are in agreement with the presence of hydrogenophosphate groups as observed in the FT-IR spectra of A-HAP.

Field emission scanning electron microscopy (FESEM) was used to observe the surface morphology of the samples (Fig. 3). FESEM showed distinct difference between two kinds of synthesized HAPs. A-HAP had amorphous morphology while hydroxyapatite crystals formed as rectangular prism in C-HAP which their size just in one dimension is in nanoscale.

2. Determination of Parameters Contribution Percentage and Optimal Removal Condition

By using Taguchi method, the optimum level for each factor was determined. To conduct an analysis of the relative importance of each factor more systematically, an analysis of variance (ANOVA) was applied to the data. The main objective of ANOVA is to extract from the results how much variations each factor causes relative to the total variation observed in the results. Contribution percentage, defined as a ratio of pure sum of the factors to the total sum of square for all factors, was calculated and presented in Table 1. According to the results the most influential factor in both removals of DR23 and AB25 was the type of process. This fact reveals basic roles of HAP type and removal method in pollutant treatment.

2-1. Effect of Type of the Process

In this study two different kinds of HAP were synthesized and two different dyes were used to study their adsorptive/photodegradation removal properties. According to the results in Fig. 4(a), A-HAP has better performance in removal of DR23 via adsorption process. This phenomenon can be explained by the poor crystalline structure of A-HAP, which increased the active surface area. In case of A-HAP exposing to UV irradiation had no obvious profit

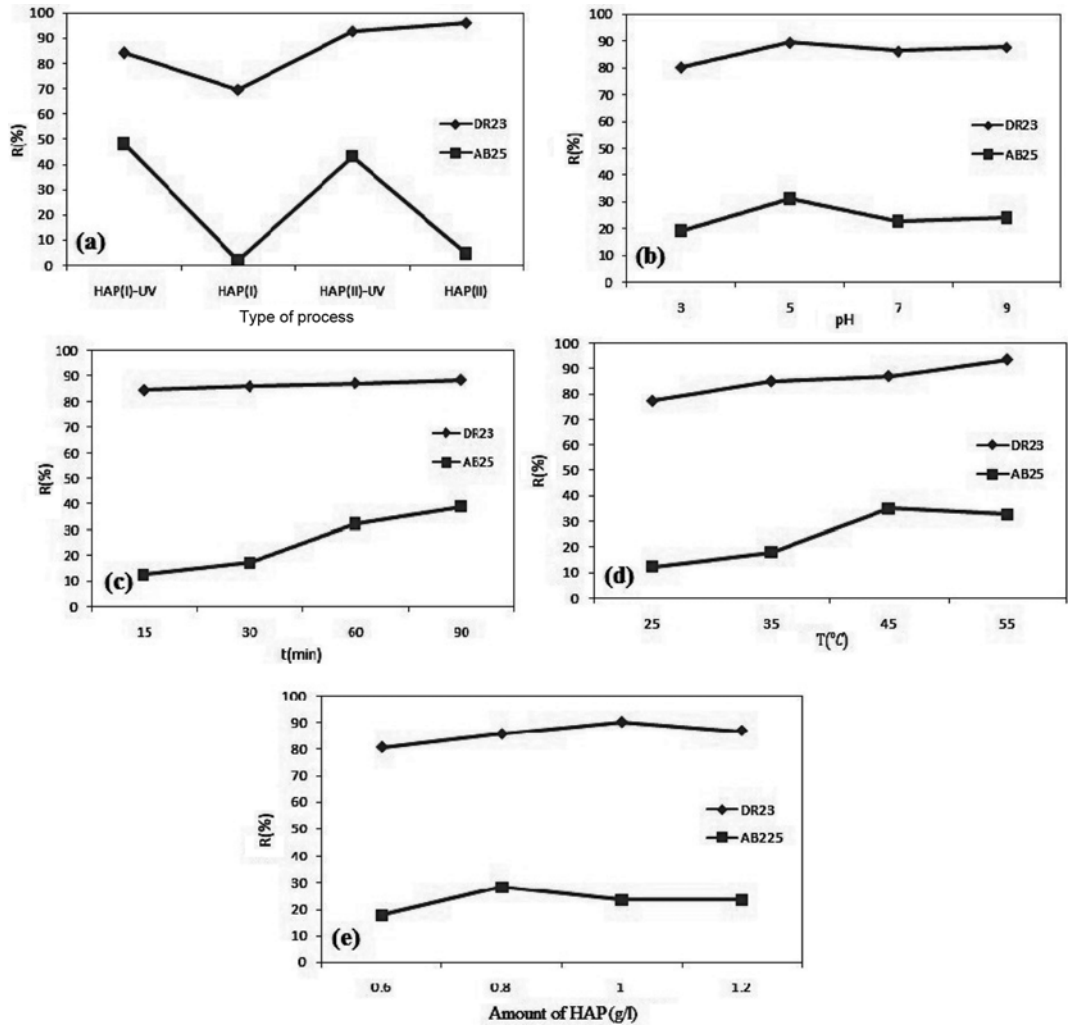

Fig. 4. Plot of the effect of each factor on the removal of DR23 and AB25.

in removal efficiency, indicating that the process is mainly adsorption phenomenon and photocatalytic degradation has not contributed efficiently in DR23 removal. As can be seen in Fig. 4(a), DR23 adsorption by C-HAP is less than A-HAP. Less adsorptive property in C-HAP gives this opportunity to photodegradation process to have a distinctive role in DR23 removal in presence of UV irradiation. In contrast with DR23, the adsorption process has not had any significant role in AB25 removal, whereas UV irradiation was initiating factor of the reaction. Among two kinds of HAP, C-HAP has shown better performance in photodegradation of AB25. The higher photoactivity of C-HAP may be caused by expansion of crystallinity in the synthesis and formation of radical species at the surface of HAP in the reaction [4].

2-2. Effect of pH

The effects of pH on the removal efficiency of DR23 and AB25, with predominant reaction of adsorption and photodegradation, are almost similar. Both HAP and Dye have functional groups, which are affected by the concentration of hydronium ions (H_3O^+-) in the solution. The removal of dyes by HAPs was studied at different initial pH of 3, 5, 7 and 9. At pH>7 and pH<3 the removal of the dye decreased. The pH of the zero charge (pH_{zc}) of the hydroxyapatite is known to be 6.8 [25]. For pH values higher than 6.8, the surface of the hydroxyapatite becomes negatively charged, while this is opposite for pH<6.8. Moreover, the dye is a weak acid; it dissociates less towards an acidic pH and is found consequently in neutral electrical form. The high removal efficiency at pH=5 as can be seen in Fig. 4(b) indicates that the positive form of hydroxyapatite is responsible for removal of both dyes. The decrease of removal efficiency in alkaline condition (pH=9) has been caused by the repulsive electrostatic forces existing between negative charged surface of hydroxyapatite and anionic groups of the dye. The decrease of removal efficiency in acidic condition can be due to the ionization of the amine and hydroxyl groups of the dye with H_3O^+ ions, which leads to positive form of dye molecules. Consequently, the repulsive electrostatic forces between positive dye and positive surface of HAP lead to removal efficiency decreasing.

2-3. Effect of Reaction Time

The dye removal efficiency of HAPs as a function of contact time is presented in Fig. 4(c). During the studies the reaction time was varied from 15 to 90 minutes. It is evident that the dye removal increases with increasing the reaction time which can be assign to increase in dye and HAP probability of encountering.

2-4. Effect of Temperature

The temperature has some major effects on the adsorptive/ degradation processes. Increasing the temperature is known to increase the diffusion rate of dye molecules across the external layer and the internal pores of the adsorbent-catalyst particles, owing to the decrease in the viscosity of the solution [15]. To study the effect of temperature on the removal of DR23 and AB25 through synthesized HAPs, we selected the following temperature: 25, 35, 45, 55 °C. Fig. 4(d) illustrates the relationship between temperature and dye removal efficiency. As can be seen, DR23 removal has increased with temperature increasing. This indicates that DR23 removal favors a high temperature. This may be a result of increase in dye mobility caused by temperature increasing. Furthermore, increasing temperature may produce a swelling effect within the internal structure of the HAP enabling dye to penetrate further. Alike to DR23 adsorption, the removal of the AB25 increased by temperature increasing. But in photocatalytic degradation system of AB25, which is based on radical formation, excess increasing of temperature, causes radicals recombination which leads to decrease radical concentration and consequently decreases degradation rate. As a result the optimized temperature for DR23 and AB25 removal was 55 °C and 45 °C, respectively.

2-5. Effect of Amount of HAP

The effect of HAP amount on dye removal is presented in Fig. 4(e). It is evident that adsorption increases with the increase in the mass of sorbent. This is due to increase in surface area and more available adsorptive sites. The same process is prospectively considered for photodegradation systems too. The removal of DR23 increased with increasing HAP quantity up to 1 g·l^{-1}. Decreasing in removal efficiency in higher HAP dosage is due to the overlapping of the active sites and agglomeration of HAP particles. For AB25, removal efficiency increased with increasing amount of catalyst up to 0.8 g·l^{-1} and then decreased. Increasing level is explained by increasing photocatalytic sites and absorbed photons. Decreasing part is clarified by agglomeration of the catalyst particles because of their small nanosizes. Another reason can be light scattering, which avoids penetration of light into inner layer of the solution [19].

3. Isotherm and Kinetic Study

The results of Taguchi experimental design revealed that the dominant process in removal of DR23 is adsorption, while photodegradation is basic process in removal of AB25. As a result for systematic study of kinetics and isotherms the outcome of Taguchi method has been applied. Since better performance of A-HAP in adsorption and higher performance of C-HAP in photodegradation, supplementary studies were done on the adsorption of DR23 on A-HAP and photodegradation of AB25 on C-HAP.

An adsorption isotherm describes the relationship between the amount of dye adsorbed at equilibrium by adsorbent and the equilibrium concentration of dye in the solution. Adsorption equilibrium provides fundamental physiochemical data for evaluating the applicability of the adsorption process as a unit operation. Isotherm behavior of DR23 adsorption on A-HAP was studied by Langmuir, Freundlich and Temkin models. The Langmuir isotherm model assumes adsorption is limited to a saturated molecular monolayer on the adsorbent surface, while the Freundlich isotherm model assumes that adsorption extended to a multilayer surface with heterogeneous energy distribution [26]. The derivation of the Temkin isotherm assumes that the fall in the heat of sorption is linear rather than logarithmic, as implied in the Freundlich equation. This isotherm considers the effects of some indirect dye/adsorbent interaction on adsorption isotherms and suggests that these interactions would decrease the heat of adsorption linearly with coverage effect of molecules in the layer [27,28]. Linearized forms of Langmuir, Freundlich and Temkin isotherms are expressed by Eq. (4), Eq. (5) and Eq. (6), respectively, and depicted in Fig. 5.

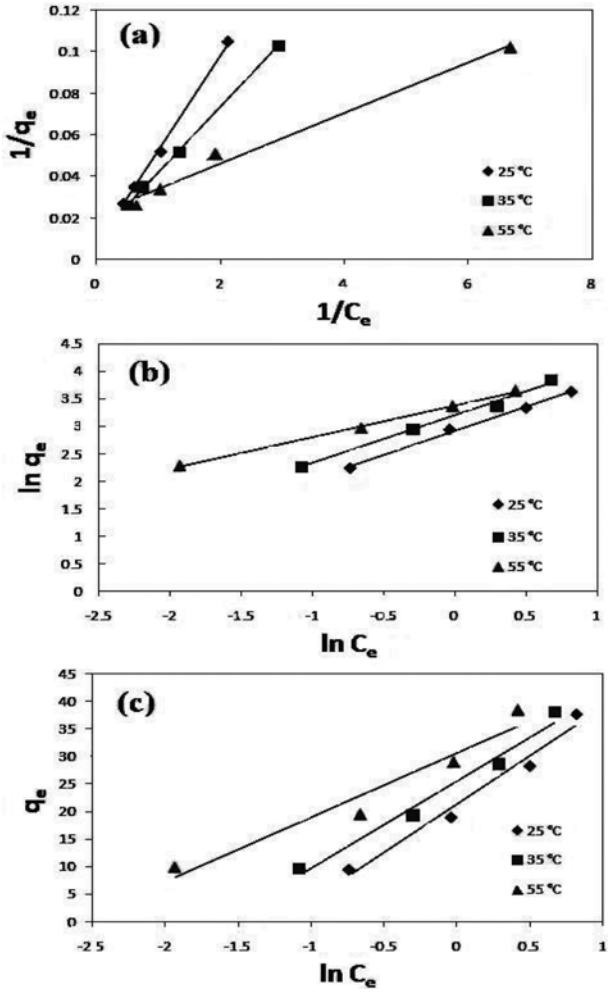

Fig. 5. Adsorption isotherms of DR23 on A-HAP at different temperature; (a) Langmuir, (b) Freundlich, (c) Temkin.

$$\frac{1}{q_e} = \frac{1}{Q_o} + \frac{1}{bQ_oC_e} \quad (4)$$

$$\ln q_e = \ln K_F + \frac{1}{n}\ln C_e \quad (5)$$

$$q_e = B\ln A + B\ln C_e \quad (6)$$

where, C_e (mg·l^{-1}) and q_e (mg·g^{-1}) are the equilibrium concentration of adsorbate in the solution and on the surface of adsorbent, respectively. Q_o (mg·g^{-1}) is the monolayer adsorption capacity, b (l·g^{-1}) is Langmuir constant which is related to the free energy of

Table 2. Isotherm constants for DR23 adsorption on A-HAP

	25 °C	35 °C	55 °C
Langmuir			
B	0.130	0.32	1.83
Q_o	166.7	100.0	45.5
R_L	0.994-0.998	0.987-0.996	0.932-0.982
R^2	0.998	0.999	0.986
X^2	493.7	236.0	49.8
Freundlich			
K_F	18.62	24.48	29.52
N	1.147	1.155	1.736
R^2	0.995	0.990	0.998
X^2	29.3	18.17	19.18
Temkin			
A	3.35	5.05	13.74
B	17.53	15.83	11.70
C	141.33	161.76	233.08
R^2	0.975	0.978	0.944

adsorption. K_F (l·mg) is the empirical constant of Freundlich isotherm and another constant of Freundlich model, n, is the empirical parameter related to the intensity of adsorption, which varies with the heterogeneity of the material. When 1/n values are in the range of 0.1<1/n<1, the adsorption process is favorable. In Temkin model B=RT/c, where T is the absolute temperature in Kelvin and R is the universal gas constant, 8.314 $J \cdot mol^{-1} \cdot K^{-1}$. The constant c is related to the heat of sorption. The calculated constants of the Langmuir, Freundlich and Temkin isotherms are given in Table 2.

Quality of the adsorption process can be expressed in term of a dimensionless separation Factor derived from Langmuir isotherm called equilibrium parameter R_L (Eq. (7)). The value of separation factor R_L indicates the adsorption process as either unfavorable (R_L>1), linear (R_L=1), favorable (0<R_L<1) or irreversible (R_L=0) [29].

$$R_L = \frac{1}{1 + bC_0} \tag{7}$$

where C_0 (mg·l^{-1}) is the initial concentration of DR23. Observed R_L factor for all adsorption temperatures was found to be less than 1 and decreased with increasing initial dye concentration. Therefore, R_L values indicated that adsorption process is favorable within this range of temperature. Addition to R_L value, the higher than unity amount of n derived from Freundlich isotherm confirmed favorable adsorption process at all studied temperatures, whereas by increasing temperature the amount of n increased too.

The correlation coefficients of both Langmuir and Freundlich isotherms are greater than 0.98. So preferring a special isotherm model for A-HAP adsorption is difficult. To solve this problem chi-square analysis according to Eq. (8) has been carried out.

$$X^2 = \sum \frac{(q_e - q_{e,m})^2}{q_{e,m}} \tag{8}$$

where $q_{e,m}$ is equilibrium capacity obtained by calculating from the model (mg·g^{-1}) and q_e is experimental data of the equilibrium capacity (mg·g^{-1}). The lower X^2 values are desired [29]. According to calculated X^2, presented in Table 2, the Freundlich isotherm model could be considered as the best fitting model for the sorption of DR23 on HAP.

Knowledge of the adsorption kinetic has an important role in study of using an adsorbent for a particular separation task. To evaluate the kinetic model of DR23 adsorption on A-HAP, the Lagergren pseudo-first-order and pseudo-second-order model were used. Since neither the first-order nor the pseudo-second-order kinetic model can identify the diffusion mechanism, the intraparticle diffusion model was also used to analyze and elucidate the diffusion mechanism. The Lagergren pseudo-first-order, pseudo-second-order and intraparticle diffusion model were represented by Eq. (9), Eq. (10) and Eq. (11) respectively [30,31].

$$\ln(q_e - q_t) = \ln q_e - K_1 t \tag{9}$$

$$\frac{t}{q_t} = \frac{1}{K_2 q_e^2} + \frac{1}{q_e} t \tag{10}$$

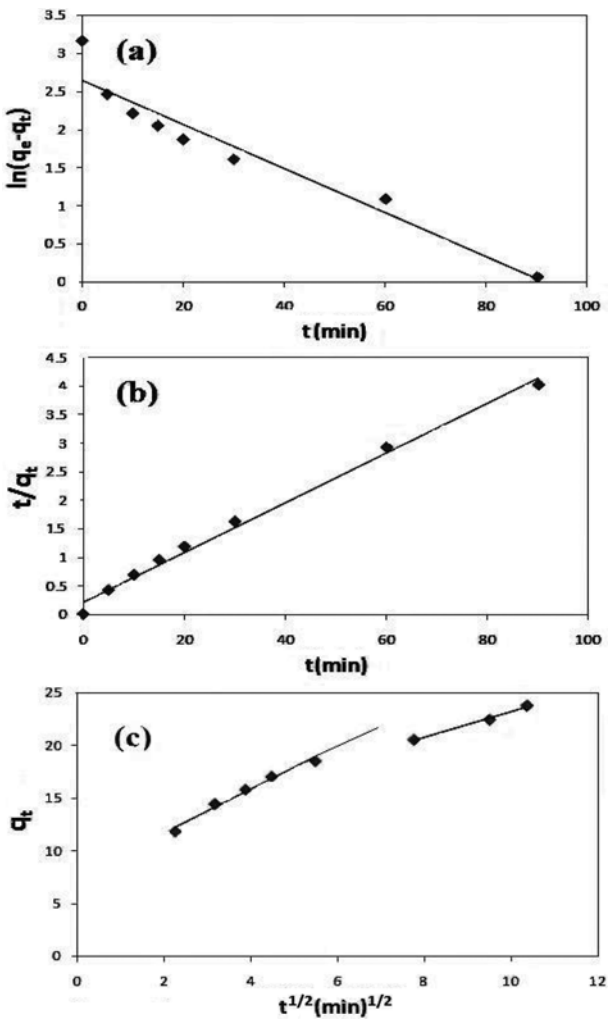

Fig. 6. Adsorption kinetic of DR23 on A-HAP; (a) Lagergren pseudo-first-order, (b) pseudo-second-order, (c) intraparticle diffusion.

Table 3. Pseudo-first-order, pseudo-second-order and intraparticle diffusion constants and coefficients for DR23 removal and Langmuir-Hinshelwood constants and coefficients for AB25 removal

Kinetic model	Parameters	
Pseudo-first-order	K_1 $(min)^{-1}$	0.028
	q_e $(mg{\cdot}g^{-1})$	14.15
	R^2	0.931
Pseudo-second-order	K_2 $(g{\cdot}mg^{-1}{\cdot}min^{-1})$	0.008
	q_e $(mg{\cdot}g^{-1})$	23.25
	R^2	0.992
Intraparticle diffusion	K_p $(mg{\cdot}g^{-1}{\cdot}min^{-1/2})$	1.374
	C $(mg{\cdot}g^{-1})$	10.05
	R^2	0.950
Langmuir-Hinshelwood	K_{obs} (min^{-1}) (10 ppm)	0.013
	R^2 (10 ppm)	0.989
	K_{obs} (min^{-1}) (20 ppm)	0.012
	R^2 (20 ppm)	0.997
	K_{obs} (min^{-1}) (30 ppm)	0.011
	R^2 (30 ppm)	0.998
	K_{obs} (min^{-1}) (40 ppm)	0.010
	R^2 (10 ppm)	0.997

$$q_t = K_p t^{1/2} + C \quad (11)$$

where K_1 (min^{-1}) and K_2 $(g{\cdot}mg^{-1}{\cdot}min^{-1})$ are the rate constants of pseudo-first-order and pseudo-second-order models and q_t $(mg{\cdot}g^{-1})$ is the amount of DR23 adsorbed at any time t (min). C $(mg{\cdot}g^{-1})$ is the intercept and K_p $(mg{\cdot}g^{-1}{\cdot}min^{-1/2})$ is the intraparticle diffusion rate constant. According to Fig. 6 the rate parameters for DR23 adsorption were obtained by drawing the linear plots of $\ln(q_e - q_t)$ versus t for the Lagergren pseudo-first-order model, t/q_t against t for the pseudo-second-order model and the q_t versus $t^{1/2}$ for the intraparticle diffusion model. The results are listed in Table 3.

It is clear to see that the R^2 value for the pseudo second-order kinetic model is much higher than that the first-order kinetic model. So the pseudo-second-order kinetic model provides a good correlation for the adsorption of DR23 onto A-HAP and suggests that the adsorption mechanism might be a physisorption process. Notably, in the intraparticle diffusion plot, the fitting line does not pass through the origin, suggesting that the adsorption of DR23 on A-HAP is a complicated process involving multiple reactions. However, the data exhibits multi-linear plots revealing that two or more steps may influence the adsorption process. The first fast step belongs to external surface adsorption and occurs so rapidly to show in the graph. The intraparticle diffusion process, which plays an important role in the adsorption of DR23, occurs in the second step. It seems the decrease of removal rate in third step is caused by DR23 concentration decreasing.

According to correlation coefficients listed in Table 3, the photocatalytic degradation of AB25by C-HAP at low initial dye concentration apparently obeys a pseudo-first-order kinetic model. The rate expression is given by Eq. (12).

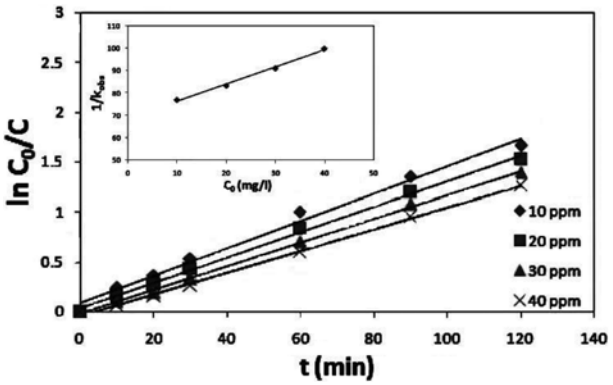

Fig. 7. The pseudo-first-order kinetic model for AB25 and plot of $1/k_{abs}$ values versus initial concentration of AB25.

$$\ln\frac{C_0}{C} = k_{obs}t \quad (12)$$

where k_{obs} (min^{-1}) is the pseudo-first order rate constant, C and C_0 $(mg{\cdot}l^{-1})$ are the concentration at time 't' and 't=0', respectively [32]. Table 3 reports the values of k_{obs} resulting from plot of $\ln(C/C_0)$ versus t for photocatalytic degradation of AB25 at different initial concentration of the dye (Fig. 7).

Adsorption is considered critical in the heterogeneous photocatalytic degradation process. This treatment is subject to the theory that sorption of the dye is a rapid equilibrium process and that the rate-determining step of the reaction is dye present in a monolayer at the solid-liquid interface. The Langmuir-Hinshelwood (L-H) isotherm, which is based on monolayer coverage of molecules, is employed to describe this adsorption step. The equation is given in the form of Eq. (13) and Eq. (14).

$$r = k_c\frac{k_{AB25}C}{1 + k_{AB25}C_0} = k_{obs}C \quad (13)$$

$$\frac{1}{k_{obs}} = \frac{1}{k_c k_{AB25}} + \frac{C_0}{k_c} \quad (14)$$

where k_{AB25} $(l{\cdot}mg^{-1})$ is the Langmuir-Hinshelwood adsorption equilibrium constant and k_c $(mg{\cdot}l^{-1}{\cdot}min^{-1})$ is the kinetic rate constant of surface reaction [32]. The variation of $1/k_{obs}$ versus C_0 should be linear. The graph based on obtained k_{obs} values (Table 3) is depicted in Fig. 7. The values of the adsorption equilibrium constant, k_{AB25}, and the kinetic rate constant of surface reaction, k_c, were calculated as 0.011 $(l{\cdot}mg^{-1})$ and 1.3 $(mg{\cdot}l^{-1}{\cdot}min^{-1})$ respectively.

CONCLUSION

The present study revealed the undeniable role of morphology and structure in effective performance of HAP in dye removal processes. FT-IR, XRD, ICP-AES, FESEM analyses were used to clarify the similarities and differences between two kinds of synthesized HAPs. The Taguchi method indicated that the type of removal process, which consists of two kinds of synthesized HAPs in the presence or absence of UV irradiation, had an important role in removal efficiency of both DR23 and AB25 dyes separately. Optimum operation conditions for removal of DR23 were found to be

A-HAP without UV irradiation at pH=5 during 90 min reaction time with the temperature of 55 °C in the presence of 1 g·l^{-1} HAP. These parameters for removal of AB25 were C-HAP exposed to UV irradiation at pH=5, during 90 min reaction time with the temperature of 45 °C and 0.8 g/*l* HAP dosage. The kinetic and isotherm studies were conducted and the results showed that the adsorption process of DR23 follows Freundlich isotherm and pseudo-second-order kinetic models. Degradation of AB25 follows Langmuir-Hinshelwood mechanism with a pseudo-first-order kinetic model. The adsorption equilibrium constant and kinetic rate constant of surface reaction for AB25 removal were 0.011 (l·mg^{-1}) and 1.3 (mg·l^{-1}·min^{-1}) respectively.

ACKNOWLEDGEMENT

The authors would like to thank the University of Zanjan for financial and other support.

REFERENCES

1. Y. Seo and J. H. Kim, *J. Ind. Eng. Chem*., **19**, 488 (2013).
2. A. Arunagiri, K. Priya, P. Kalaichelvi and R. Anantharaj, *J. Ind. Eng. Chem*., **20**, 2409 (2014).
3. M. Asadullah, M. Kabir, M. Ahmed, N. Razak, N. Rasid and A. Aezzira, *Korean J. Chem. Eng*., **30**, 2228 (2013).
4. A. Safavi and S. Momeni, *J. Hazard. Mater*., **201-202**, 125 (2012).
5. B. Thongrom, P. Amornpitoksuk, S. Suwanboon and J. Baltrusaitis, *Korean J. Chem. Eng*., **31**, 587 (2014).
6. L. Kong, Z. Zhang, H. Xing, Q. Yang, B. Su, Z. Bao, Y. Yang and Q. Ren, *Korean J. Chem. Eng*., **32**, 511 (2015).
7. B. K. Körbahti, K. Artut, C. Geçgel and A. Özer, *Chem. Eng. J*., **173**, 677 (2011).
8. M. T. Yagub, T. K. Sen, S. Afroze and H. M. Ang, *Adv. Colloid Interface Sci*., **209**, 172 (2014).
9. A. R. Khataee, M. Zarei and R. Ordikhani-Seyedlar, *J. Mol. Catal. A-Chem*., **338**, 84 (2011).
10. S. Chowdhury and R. Balasubramanian, *Appl. Catal. B-Environ*., **160-161**, 307 (2014).
11. A. Nezamzadeh-Ejhieh and H. Zabihi-Mobarakeh, *J. Ind. Eng. Chem*., **20**, 1421 (2014).
12. B. Nasiri-Tabrizi, A. Fahami and R. Ebrahimi-Kahrizsangi, *J. Ind. Eng. Chem*., **20**, 245 (2014).
13. F. Perut, E. B. Montufar, G. Ciapetti, M. Santin, J. Salvage, T. Traykova, J. A. Planell, M. P. Ginebra and N. Baldini, *Acta Biomater*., **7**, 1780 (2011).
14. L. M. Svanborg, M. Hoffman, M. Andersson, F. Currie, P. Kjellin and A. Wennerberg, *Int. J. Oral Maxillofac. Surg*., **40**, 308 (2011).
15. N. Barka, S. Qourzal, A. Assabbane, A. Nounah and Y. AÎT-Ichou, *J. Environ. Sci*., **20**, 1268 (2008).
16. S. Chun, S. An, S. Lee, J. Kim and S. Chang, *Korean J. Chem. Eng*., **31**, 994 (2014).
17. J. H. Shariffuddin, M. I. Jones and D. A. Patterson, *Chem. Eng. Res. Des*., **91**, 1693 (2013).
18. W. P. S. L. Wijesinghe, M. M. M. G. P. G. Mantilaka, E. V. A. Premalal, H. M. T. U. Herath, S. Mahalingam, M. Edirisinghe, R. P. V. J. Rajapakse and R. M. G. Rajapakse, *Mater. Sci. Eng*., **42**, 83 (2014).
19. Z.-p. Yang, X.-y. Gong and C.-j. Zhang, *Chem. Eng. J*., **165**, 117 (2010).
20. S. Aber, D. Salari and M. R. Parsa, *Chem. Eng. J*., **162**, 127 (2010).
21. T. Mohammadi and M. A. Safavi, *Desalination*, **249**, 83 (2009).
22. H. Nishikawa and K. Omamiuda, *J. Mol. Catal. A-Chem*., **179**, 193 (2002).
23. G. E. J. Poinern, M. K. Ghosh, Y.-J. Ng, T. B. Issa, S. Anand and P. Singh, *J. Hazard. Mater*., **185**, 29 (2011).
24. C. Stötzel, F. A. Müller, F. Reinert, F. Niederdraenk, J. E. Barralet and U. Gbureck, *Colloids Surf., B*., **74**, 91 (2009).
25. M. P. Reddy, A. Venugopal and M. Subrahmanyam, *Appl. Catal. B-Environ*., **69**, 164 (2007).
26. X. Yu, S. Tong, M. Ge and J. Zuo, *Carbohydr. Polym*., **92**, 269 (2013).
27. V. M. Vučurović, R. N. Razmovski, U. D. Miljić and V. S. Puškaš, *J. Taiwan Inst. Chem. E*., **45**, 1700 (2014).
28. E. Malkoc, *J. Hazard. Mater*., **137**, 899 (2006).
29. A. Mirmohseni, M. S. Seyed Dorraji, A. Figoli and F. Tasselli, *Bioresour. Technol*., **121**, 212 (2012).
30. M. Mourabet, A. El Rhilassi, H. El Boujaady, M. Bennani-Ziatni, R. El Hamri and A. Taitai, *J. Saudi Chem. Soc*. (2012), DOI:10.1016/j.jscs.2012.03.003.
31. K. Lin, J. Pan, Y. Chen, R. Cheng and X. Xu, *J. Hazard. Mater*., **161**, 231 (2009).
32. N. Daneshvar, M. H. Rasoulifard, A. R. Khataee and F. Hosseinzadeh, *J. Hazard. Mater*., **143**, 95 (2007).